ChemPubSoc Europe

DOI: 10.1002/cbic.201900110

CHEMBIOCHEM Communications

Design of an Ultrafast G Protein Switch Based on a Mouse Melanopsin Variant

Stefan Alexander Tennigkeit[+],[a] Raziye Karapinar[+],[b] Till Rudack[+],[a] Max-Aylmer Dreier,[a] Philipp Althoff,[a] Dennis Eickelbeck,[b] Tatjana Surdin,[b] Michelle Grömmke,[b] Melanie D. Mark,[b] Katharina Spoida,[b] Mathias Lübben,[a] Udo Höweler,[c] Stefan Herlitze,*[b] and Klaus Gerwert*[a]

The primary goal of optogenetics is the light-controlled noninvasive and specific manipulation of various cellular processes. Herein, we present a hybrid strategy for targeted protein engineering combining computational techniques with electrophysiological and UV/visible spectroscopic experiments. We validated our concept for channelrhodopsin-2 and applied it to modify the less-well-studied vertebrate opsin melanopsin. Melanopsin is a promising optogenetic tool that functions as a selective molecular light switch for G protein-coupled receptor pathways. Thus, we constructed a model of the melanopsin G_q protein complex and predicted an absorption maximum shift of the Y211F variant. This variant displays a narrow blue-shifted action spectrum and twofold faster deactivation kinetics compared to wild-type melanopsin on G protein-coupled inward rectifying K^+ (GIRK) channels in HEK293 cells. Furthermore, we verified the in vivo activity and optogenetic potential for the variant in mice. Thus, we propose that our developed concept will be generally applicable to designing optogenetic tools.

Light is vital for most living organisms. The ability to sense and respond to light is mediated by different light-sensitive proteins.[1] Optogenetics is an innovative technique combining the use of light-sensitive proteins and genetically targeted cells in organisms to precisely perform light-controlled manipulation of cell function and signaling.[2] A prerequisite for the targeted engineering of light-sensitive proteins to be used as precise noninvasive optogenetic tools is a detailed atomistic understanding of photoactivatable biological processes.

[a] S. A. Tennigkeit,[+] T. Rudack,[+] M.-A. Dreier, P. Althoff, M. Lübben, Prof. Dr. K. Gerwert
Department of Biophysics, Ruhr University Bochum
Universitätsstrasse 150, 44780 Bochum (Germany)
E-mail: klaus.gerwert@bph.rub.de

[b] R. Karapinar,[+] D. Eickelbeck, T. Surdin, M. Grömmke, M. D. Mark, K. Spoida, Prof. Dr. S. Herlitze
Department of General Zoology and Neurobiology, Ruhr University Bochum
Universitätsstrasse 150, 44780 Bochum (Germany)
E-mail: sxh106@gmail.com

[c] U. Höweler
Westfälische Wilhelms-Universität Münster, Organisch-Chemisches Institut
Corrensstrasse 40, 48149 Münster (Germany)

[+] These authors contributed equally to this work.

Supporting information and the ORCID identification numbers for the authors of this article can be found under https://doi.org/10.1002/cbic.201900110.

By now microbial rhodopsins are the best-studied optogenetic tools.[3,4] Bacteriorhodopsin (bR),[5] the first discovered representative of this class, inspired the development of novel biophysical tools for structural and functional investigation. Microbial rhodopsins span the membrane by seven transmembrane helices and comprise the chromophore retinal, which is covalently bound to a lysine through a protonated Schiff base. Fundamental research has enabled us to understand the structure and function of bR[6,7] and paved the way for studies of many additional microbial rhodopsins. Among these is the currently most widely used optogenetic tool channelrhodopsin-2 (ChR2), a light-gated ion channel from *Chlamydomonas reinhardtii* belonging to the type I opsins.[3,4,8] Since the usefulness of ChR2 in optogenetics has been established, many improved variants have been designed.[9,10]

Other key players in optogenetics are type II (animal) opsins belonging to the family of G protein-coupled receptors (GPCRs). Once activated by light, the GPCR in complex with specific G proteins activates second messengers and signaling pathways to control a variety of vital physiological processes, for example, vision.[11] We have studied the photoreceptor GPCR melanopsin from vertebrates, which occurs in intrinsically photosensitive retinal ganglion cells (ipRGCs) being mainly involved in nonvision processes.[12,13]

In optogenetic experiments, melanopsin operates as a selective molecular switch with limited phototoxicity. It is a tristable opsin that enables a precise control of the activation and deactivation of GPCR pathways and/or neuronal firing,[14,15] which is switched on by blue light and off by yellow light.[16] G protein transduction is divided into two classes: the cAMP signal pathway and phosphatidylinositol bisphosphate (PIP_2) pathway. G_i inhibits the cAMP signal pathway and G_q activates the PIP_2 pathway. Whereas vertebrate ciliary photoreceptors usually activate the G_t pathway,[17] melanopsin is one of the few known vertebrate opsins to be capable of activating $G_{q/11}$ signaling in neurons. Other light-activated GPCRs are vertebrate cone opsins (i.e., short-wave (vSWO) and long-wave (vLWO) opsins), which solely activate the $G_{i/o}$ pathway. vSWO- and vLWO-mediated $G_{i/o}$ pathway activation in neurons are maximally induced by UV light and red light, respectively,[18] whereas melanopsin-mediated $G_{q/11}$ pathway activation in neurons is maximally induced by blue light.[19]

A long-term goal is to specifically light activate and deactivate distinct G protein-coupled pathways by using melanopsin in parallel with a distinct vertebrate opsin expressed in the

© 2019 Wiley-VCH Verlag GmbH & Co. KGaA, Weinheim

same cell. However, crosstalk between the absorption bands of melanopsin and cone opsins might exist. To optimize the optogenetic performance of melanopsin in combination with cone opsins for in vivo applications, the excitation overlap of these proteins has to be eliminated by engineering a +melanopsin variant with blue-shifted activation spectrum (Figure S1 in the Supporting Information). However, changing the wavelength dependency ("color tuning") of melanopsin by trial-and-error experimental methods usually involves tedious human work. Therefore, a knowledge-based approach considering the structure–wavelength relationship is desired to lead to a systematic protein-engineering strategy that reduces human work for color tuning.

Biomolecular simulations are a useful tool to gain information for such a systematic strategy. In fact, the introduction of hybrid quantum mechanics and molecular mechanics (QM/MM) simulations[20] enabled the first calculated UV/Vis spectrum and color-tuning studies of the retinal protein bR,[21] ChR2,[22] and of melanopsin.[23] Theoretical UV/Vis spectroscopy allows the calculation of excitation energies, provided that structural models of the involved proteins are accessible. In order to obtain a reliable prediction of the structure–wavelength relationship for targeted color tuning, a careful validation of the UV/Vis calculation approach is needed. Especially as there is a huge variety of conceptually different approaches (semi-empirical or density functional theory (DFT)) to set up and calculate excitation energies; the determination of the appropriate approach is of particular importance.[24] Therefore, in this work, we first used the well-studied ChR2[3,4,8,25,26] to validate and establish our UV/Vis spectra calculation workflow, which then enabled us to predict a melanopsin variant with shifted absorption maximum (λ_{max}).

Initially, we identified putative mutations for a red-shifted λ_{max} of ChR2, because the radiation of red light is less harmful to tissue and has a deeper penetration depth. Figure S2A shows the sequence alignment of several microbial rhodopsins, for example, Chrimson,[27] which are known to have a red-shifted λ_{max} compared to ChR2.[5,28–30] Combining this sequence information with the structural information from the ChR2 X-ray structure (PDB ID: 6EID;[31] Figure S2B), we considered only those residues in close proximity to the retinal. Our analysis yielded four novel ChR2 variants (K93F, G181S, S256A and K93F/S256A; Figure 1A) not yet discussed in the literature. These variants affect the local polarity within the retinal binding pocket. We made UV/Vis spectroscopic measurements to demonstrate that all these mutants have a red-shifted λ_{max} (Figure 1B and Table 1).

Concurrent λ_{max} shifts of the ChR2 variants described above were calculated by employing the theoretical UV/Vis spectroscopy workflow detailed in Supporting Note 1 and in Figure S4. The recently resolved X-ray structure of ChR2[31] was used as the initial structural model. Excitation energies were calculated by using three different conceptual approaches; the semi-empirical CI method with modified neglect of diatomic overlap (MNDOC) parameters[32] and two different DFT approaches, namely TD/631-G*, and RCIS=(FC)/6-31G*.[24] The measured and calculated λ_{max} shifts are compared in Table 1, which reveals that all methods predict a red shift of the ChR2 mutants; this is in full accordance with the experiment (Figure 1B). Therefore, from here on, we used only the fastest and computationally cheapest semiempirical CI method with MNDOC parameters available to us; this allows for the necessary QM/MM coupling.

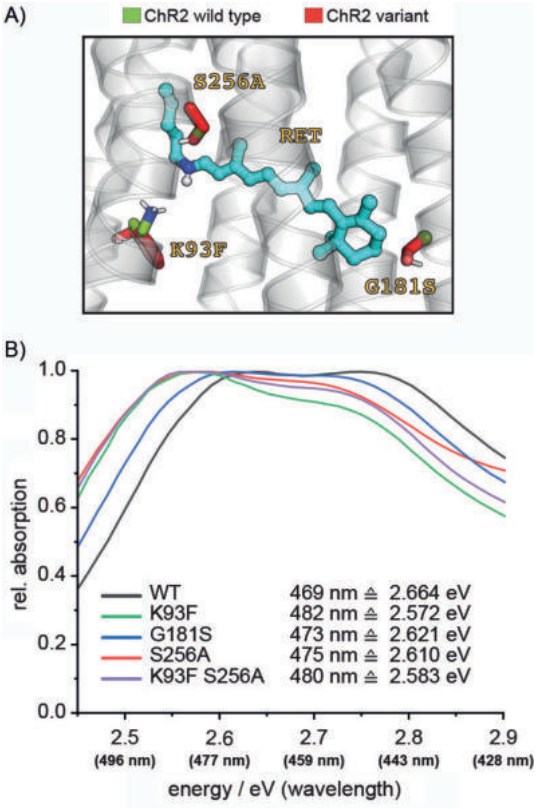

Figure 1. UV/Vis spectroscopy of ChR2 variants. A) The ChR2 all-*trans* retinal (cyan) binding pocket, based on PDB ID: 6EID,[31] with site-specific variants highlighted. B) The experimentally determined absorption spectra of all ChR2 variants were red-shifted with respect to that of WT. See also Figure S3 and Table 1.

Table 1. Measured and calculated UV/Vis absorption shifts of ChR2 wild-type and site-specific variants. The average shifts of both monomers are given; absolute values are presented in Table S1.

	UV/Vis absorption shifts [eV]			
	Measured	MNDOC	TD/6-31G*	RCIS=(FC)/6-31G*
G181S	−0.022	−0.019	−0.030	−0.030
S256A	−0.034	−0.039	−0.038	−0.037
K93F	−0.072	−0.043	−0.029	−0.030
K93F/S256A	−0.061	−0.049	−0.043	−0.042

Our theoretical UV/Vis spectroscopy approach enables us to predict the shift direction of the absorption maximum of variants. Through this prediction, we reduce the number of experimentally measured variants to a small pool of promising candidates. Such targeted selection of candidates is more economic than strictly random trial-and-error experiments.

Correct prediction of the structure–wavelength relation strongly depends on the quality of the structural model used

© 2019 Wiley-VCH Verlag GmbH & Co. KGaA, Weinheim

to initiate the excitation energy calculations. In contrast to ChR2, the 3D structure of melanopsin has not yet been experimentally determined. However, recent breakthroughs in structural biology allowed structural models of opsins to be obtained by X-ray crystallography,[33–35] cryo-electron microscopy,[36,37] and homology modeling.[23] Using these structural data, we constructed an atomistic model of membrane-inserted solvated melanopsin G_q protein complex. As outlined in Supporting Note 2 and Figure S5, we optimized the modeling concept, which was initially developed to build soluble proteins like the proteasome,[38] to create structural models of transmembrane proteins. The key benefit of this concept is to streamline and facilitate the use of established but often complicated modeling suites like Rosetta and Modeller for ab initio structure prediction and homology modeling.

For homology modeling of free melanopsin (i.e., not in complex with G proteins), we chose the same template as Sekharan et al.,[23] a squid rhodopsin.[34] However, the model of Sekharan et al. erroneously introduced an extra isoleucine into the mouse melanopsin sequence at position 129. Our corrected sequence alignment is shown in Figure 2A. Figure 2B reveals that the similarity between melanopsin and squid rhodopsin is sufficient to build a reliable model exhibiting a similarity of 68% within the modeled sequence region. Table S2 reflects that within the retinal binding pocket region (all amino acids within 10 Å distance of the retinal) the sequence similarity reaches 79%. A correct assignment is further ensured by the marked anchor residues (Figure 2A) considered to be residues in the helical region that are identical in the sequence alignment. The helical regions, highlighted in green, were identified by using a variety of different computational tools, as outlined in Figure S6.

Next, the melanopsin G_q protein complex was modeled as detailed in the Supporting Note 2: The X-ray structure of β_2AR in complex with the G_s protein[33] served as the basis for the binary complex model (Figures S7 and S8). The resulting struc-

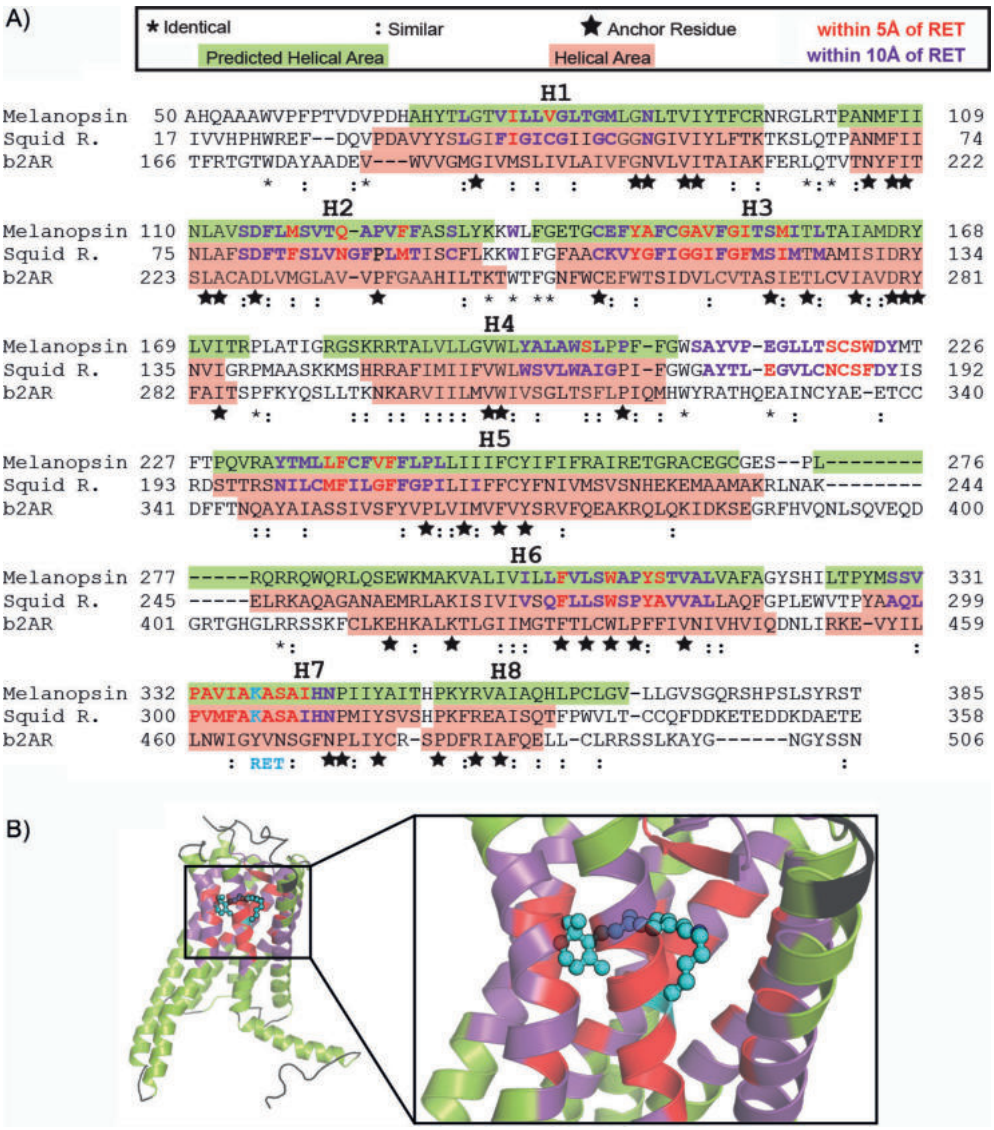

Figure 2. Melanopsin model construction. A) Sequence alignment of melanopsin with squid rhodopsin[34] and β_2AR.[33] The residues within 5 Å of the retinal are written in red and those 5–10 Å from retinal are in purple. The predicted helices are highlighted in green (Figure S6), and the helical residues of the X-ray structures are in pink. B) Final melanopsin homology model.

© 2019 Wiley-VCH Verlag GmbH & Co. KGaA, Weinheim

ture was then used to initiate a 100 ns molecular mechanics (MM) equilibration. In five subsequent independent MM production runs (100 ns each), the protein-backbone-forming Cα atom positions converged as shown by their root mean square deviations (RMSD; Figure S9). Thus, we consider the structural model obtained to be stable and reliable.

To calculate the theoretical UV/Vis spectra, we adopted the approach we used for ChR2, starting by identifying hot spots for amino acid exchange in melanopsin. Here, we focused on the residues in the area between 5 and 10 Å from retinal (Figure S10). These residues are close enough to the retinal to have a significant electrostatic influence; however, they are also likely far enough away to keep the overall structure and function of melanopsin intact. We identified Y211F (Figure 4A) as a promising variant for which we calculated a blue-shifted λ_{max} of +0.016 eV.

We characterized the biophysical, optogenetic properties of Y211F melanopsin by using patch-clamp recordings in HEK293 cells with stable expressing G protein-coupled inward rectifying K^+ (GIRK) 1,2 channels. In these cells, light-activated melanopsins result in a $G_{i/o}$-pathway-mediated GIRK current. (Note, in neurons melanopsin activates mainly the $G_{q/11}$ pathway, whereas in HEK293 cells it activates the $G_{i/o}$ and the $G_{q/11}$ pathways.[16]) As predicted, the Y211F variant reveals a blue-shifted λ_{max} in the activation action spectrum at 450 nm (2.755 eV) compared to 470 nm (2.638 eV) for WT melanopsin (Figure 3 and the Supporting Note 3). The action spectrum (Figure 3B) reveals a narrower shape for Y211F than for the WT. Both completely deactivate GIRK currents at 560 nm (2.214 eV, Figure S11). The resulting 20 nm (0.117 eV) shift during light-induced activation is somewhat larger than predicted.

Furthermore, we characterized the activation and deactivation of melanopsin-induced GIRK currents (Figure 3C and D). The activation and deactivation kinetics determine how fast a cellular pathway can be controlled by light. The melanopsin-dependent, light-induced GIRK current activation and deactivation of variant Y211F ($\tau_{on} \approx 1.0$ s; $\tau_{off} \approx 5.0$ s) are faster than in WT melanopsin ($\tau_{on} \approx 1.4$ s; $\tau_{off} \approx 8.9$ s). The Y211F variant also reveals a transient activation of the G protein pathways (Figure 3C), as becomes obvious in the 45% decline in response amplitude for Y211F in comparison to for WT (15%) when melanopsins are deactivated after 30 s (Figures 3C and S12A, B).

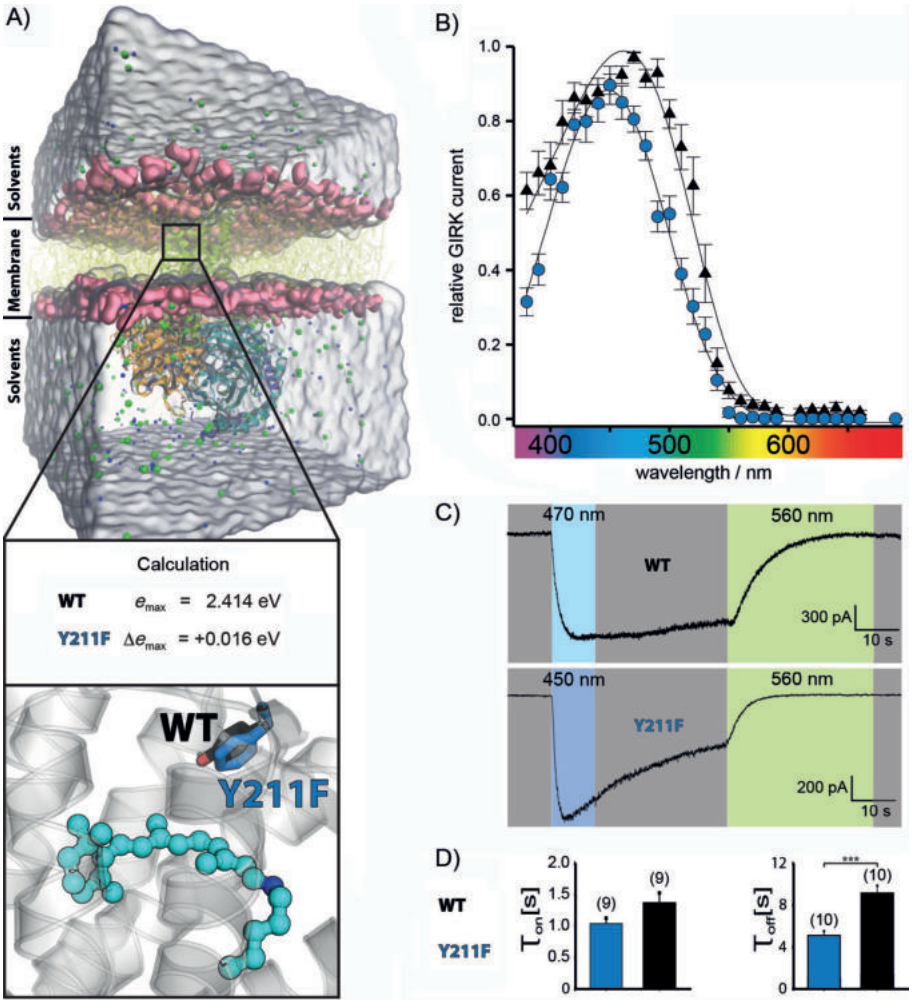

Figure 3. In silico and in vitro characterization of the Y211F variant. A) Simulation system of the melanopsin G_q protein complex with the retinal binding pocket enlarged and the calculated λ_{max} shift of the Y211F variant. B) Wavelength dependency of a normalized light-induced GIRK currents evoked by WT (▲) and Y211F (●) activation ($n = 7$ cells). C) Comparison of GIRK current traces induced by WT and Y211F. D) Comparison of the activation (τ_{on}, $n = 9$ cells) and deactivation (τ_{off}, $n = 10$ cells) time constants of Y211F and WT melanopsin.

© 2019 Wiley-VCH Verlag GmbH & Co. KGaA, Weinheim

However, light-activated, Y211F-mediated responses do not decline in amplitude when deactivation occurs immediately after activation. This allows for repetitive, fast, long-term stimulation of the G protein pathway (Figure S13A), which is currently not possible with other melanopsin variants.[16] The fast temporal control of the G protein pathway is possible because of the fast activation and deactivation kinetics of Y211F (Figure 3D). Thus, Y211F is an ideal tool to control intracellular G protein signals repetitively with very low phototoxicity. (For a detailed characterization of our variant see Supporting Note 4 and Figures S11–S15.)

We next analyzed the potential of combining our tuned melanopsin variant with $G_{i/o}$-pathway-activating vertebrate cone opsins for simultaneous optogenetic control of two independent G protein pathways in vivo. As it has a narrow action spectrum, Y211F can be combined with vertebrate $G_{i/o}$ coupled short-wave opsin (vSWO) and long-wave opsin (vLWO). As shown in Figure 4A vSWO can be activated at 380 nm (100% activity) with negligible crosstalk with Y211F melanopsin, which is only 31% active, compared to 61% of WT. Equally, activation of Y211F at 480 nm (75%) leads to negligible activation of vSWO (20%). On the other hand, Y211F can be activated at 420 nm (80%) with negligible crosstalk with vLWO activation (<30%; Figure 4B). Y211F can be deactivated at 560 nm without activation of Y211F (0%) or vSWO (0%; Figure 4A), but with strong activation of vLWO (>75%; Figure 4B). Thus, combining Y211F melanopsin either with vSWO or vLWO is a promising optogenetic strategy for the specific activation and deactivation of different G protein pathways in vivo.

As a first step towards in vivo application, we demonstrated that Y211F optogenetically controls neuronal firing. We expressed Y211F specifically in Purkinje cells (PC; Figure 5A), an important neuron type in the cerebellum for integrating motor commands and adjusting motor behavior. As shown in Figure 5, 10 s pulses of blue light increase the firing frequency of PC. These proof-of-principle experiments demonstrate a promising optogenetic potential for in vivo application of the Y211F melanopsin variant.

In conclusion, we have presented a hybrid concept for targeted protein engineering. We have established a UV/Vis spectra calculation workflow and constructed a homology model of the melanopsin G_q protein complex. With this approach, we identified the Y211F melanopsin variant. Electrophysiological experiments revealed that the variant exhibits enhanced temporal precision for controlling G protein signals, with faster activation and twofold faster deactivation kinetics than WT mela-

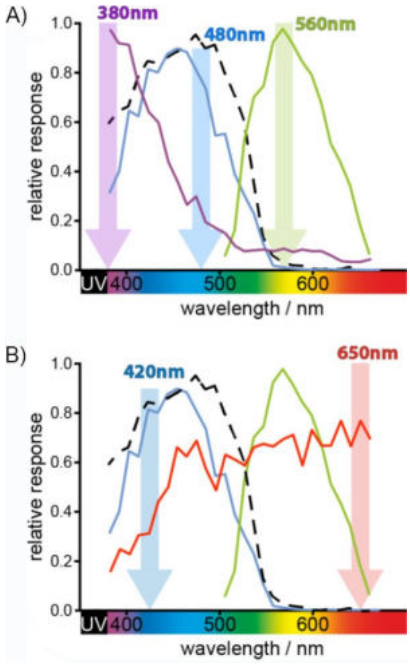

Figure 4. Potential optogenetic application of Y211F melanopsin. A) Distinct activation of vSWO (——) at 380 nm as well as Y211F (——) at 480 nm and deactivation of Y211F (——) at 560 nm with negligible excitation energy overlap. B) The transient character of the Y211F melanopsin variant now allows its combination with vLWO (——), as it does not need to be switched off anymore; Y211F melanopsin can be activated at 420 nm and vLWO at 650 nm. vLWO and vSWO data are from our previous publication.[18] All graphs represent normalized light induced GIRK currents; WT (-----) is shown for comparison.

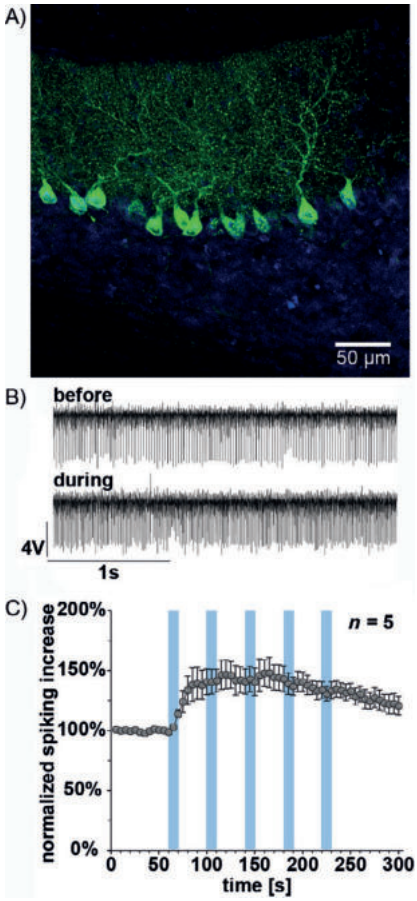

Figure 5. In vivo characterization of Y211F melanopsin. A) Adeno-associated virus (AAV)-mediated expression of yellow fluorescent protein (YFP)-tagged Y211F melanopsin (green) in cerebellar Purkinje cells. Blue shows where the PCs are stained with Nissl. B) Example in vivo traces of spiking cerebellar PC before and during light application. C) activation of Y211F expressed in cerebellar PCs by 10 s pulses of light (■) increases the firing frequency of PCs. Average: change in normalized firing frequency of five cells of one mouse.

© 2019 Wiley-VCH Verlag GmbH & Co. KGaA, Weinheim

nopsin. In addition, the narrow action spectrum makes our variant a promising candidate for combined activation with the cone opsins vSWO and vLWO for specific activation and deactivation of different G protein pathways in the brain and other tissues.

Acknowledgements

We thank Gabi Smuda for technical support, the Deutsche Forschungsgemeinschaft He2471/23-1, He2471/21-1, He2471/19-1 Priority Program (SPP1926), SFB874 (B10), SFB1280 (A07), Deutsche Studiensstiftung, and the Friedrich-Ebert-Stiftung for financial support.

Conflict of Interest

The authors declare no conflict of interest.

Keywords: computational chemistry · electrophysiology · integrative modeling · mutagenesis · structural biology

[1] O. P. Ernst, D. T. Lodowski, M. Elstner, P. Hegemann, L. S. Brown, H. Kandori, *Chem. Rev.* **2014**, *114*, 126 – 163.
[2] K. Deisseroth, *Nat. Methods* **2011**, *8*, 26 – 29.
[3] E. S. Boyden, F. Zhang, E. Bamberg, G. Nagel, K. Deisseroth, *Nat. Neurosci.* **2005**, *8*, 1263 – 1268.
[4] G. Nagel, T. Szellas, W. Huhn, S. Kateriya, N. Adeishvili, P. Berthold, D. Ollig, P. Hegemann, E. Bamberg, *Proc. Natl. Acad. Sci. USA* **2003**, *100*, 13940 – 13945.
[5] D. Oesterhelt, W. Stoeckenius, *Nat. New Biol.* **1971**, *233*, 149 – 152.
[6] K. Gerwert, B. Hess, J. Soppa, D. Oesterhelt, *Proc. Natl. Acad. Sci. USA* **1989**, *86*, 4943 – 4947.
[7] F. Garczarek, K. Gerwert, *Nature* **2006**, *439*, 109 – 112.
[8] X. Li, D. V. Gutierrez, M. G. Hanson, J. Han, M. D. Mark, H. Chiel, P. Hegemann, L. T. Landmesser, S. Herlitze, *Proc. Natl. Acad. Sci. USA* **2005**, *102*, 17816 – 17821.
[9] J. Y. Lin, M. Z. Lin, P. Steinbach, R. Y. Tsien, *Biophys. J.* **2009**, *96*, 1803 – 1814.
[10] J. Y. Lin, *Exp. Physiol.* **2011**, *96*, 19 – 25.
[11] S. Hughes, M. W. Hankins, R. G. Foster, S. N. Peirson in *Progress in Brain Research* (Eds.: A. Kalsbeek, M. Merrow, T. Roenneberg, R. G. Foster), Elsevier, **2012**, pp. 19 – 40.
[12] S. Herlitze, L. T. Landmesser, *Curr. Opin. Neurobiol.* **2007**, *17*, 87 – 94.
[13] M. W. Hankins, S. N. Peirson, R. G. Foster, *Trends Neurosci.* **2008**, *31*, 27 – 36.
[14] A. J. Emanuel, M. T. H. Do, *Neuron* **2015**, *85*, 1043 – 1055.
[15] K. Spoida, O. A. Masseck, E. S. Deneris, S. Herlitze, *Proc. Natl. Acad. Sci. USA* **2014**, *111*, 6479 – 6784.
[16] K. Spoida, D. Eickelbeck, R. Karapinar, T. Eckhardt, M. D. Mark, D. Jancke, B. V. Ehinger, P. König, D. Dalkara, S. Herlitze, O. A. Masseck, *Curr. Biol.* **2016**, *26*, 1206 – 1212.
[17] Y. Shichida, H. Imai, *Cell. Mol. Life Sci.* **1998**, *54*, 1299 – 1315.
[18] O. A. Masseck, K. Spoida, D. Dalkara, T. Maejima, J. M. Rubelowski, L. Wallhorn, E. S. Deneris, S. Herlitze, *Neuron* **2014**, *81*, 1263 – 1273.
[19] S. Panda, S. K. Nayak, B. Campo, J. R. Walker, J. B. Hogenesch, T. Jegla, *Science* **2005**, *307*, 600 – 604.
[20] A. Warshel, M. Levitt, *J. Mol. Biol.* **1976**, *103*, 227 – 249.
[21] M. Hoffmann, M. Wanko, P. Strodel, P. H. König, T. Frauenheim, K. Schulten, W. Thiel, E. Tajkhorshid, M. Elstner, *J. Am. Chem. Soc.* **2006**, *128*, 10808 – 10818.
[22] A. Ardevol, G. Hummer, *Proc. Natl. Acad. Sci. USA* **2018**, *115*, 3557 – 3562.
[23] S. Sekharan, J. N. Wei, V. S. Batista, *J. Am. Chem. Soc.* **2012**, *134*, 19536 – 19539.
[24] H. M. Senn, W. Thiel, *Angew. Chem. Int. Ed.* **2009**, *48*, 1198 – 1229; *Angew. Chem.* **2009**, *121*, 1220 – 1254.
[25] K. Eisenhauer, J. Kuhne, E. Ritter, A. Berndt, S. Wolf, E. Freier, F. Bartl, P. Hegemann, K. Gerwert, *J. Biol. Chem.* **2012**, *287*, 6904 – 6911.
[26] J. Kuhne, K. Eisenhauer, E. Ritter, P. Hegemann, K. Gerwert, F. Bartl, *Angew. Chem. Int. Ed.* **2015**, *54*, 4953 – 4957; *Angew. Chem.* **2015**, *127*, 5037 – 5041.
[27] K. Oda, J. Vierock, S. Oishi, S. Rodriguez-Rozada, R. Taniguchi, K. Yamashita, J. S. Wiegert, T. Nishizawa, P. Hegemann, O. Nureki, *Nat. Commun.* **2018**, *9*, 3949.
[28] N. C. Klapoetke, Y. Murata, S. S. Kim, S. R. Pulver, A. Birdsey-Benson, Y. K. Cho, T. K. Morimoto, A. S. Chuong, E. J. Carpenter, Z. Tian, et al., *Nat. Methods* **2014**, *11*, 338 – 346.
[29] B. S. Krause, C. Grimm, J. C. D. Kaufmann, F. Schneider, T. P. Sakmar, F. J. Bartl, P. Hegemann, *Biophys. J.* **2017**, *112*, 1166 – 1175.
[30] J. Y. Lin, P. M. Knutsen, A. Muller, D. Kleinfeld, R. Y. Tsien, *Nat. Neurosci.* **2013**, *16*, 1499 – 1508.
[31] O. Volkov, K. Kovalev, V. Polovinkin, V. Borshchevskiy, C. Bamann, R. Astashkin, E. Marin, A. Popov, T. Balandin, D. Willbold, G. Büldt, E. Bamberg, V. Gordeliy, *Science* **2017**, *358*, eaan8862.
[32] W. Thiel, *J. Am. Chem. Soc.* **1981**, *103*, 1413 – 1420.
[33] S. G. F. Rasmussen, B. T. DeVree, Y. Zou, A. C. Kruse, K. Y. Chung, T. S. Kobilka, F. S. Thian, P. S. Chae, E. Pardon, D. Calinski, et al., *Nature* **2011**, *477*, 549 – 555.
[34] M. Murakami, T. Kouyama, *Nature* **2008**, *453*, 363 – 367.
[35] M. E. Sommer, M. Elgeti, P. W. Hildebrand, M. Szczepek, K. P. Hofmann, P. Scheerer in *Methods in Enzymology, Vol. 556: **Membrane Proteins**: Production and Functional Characterization* (Ed.: A. K. Shukla), Academic Press, San Diego, **2015**, pp. 563 – 608.
[36] Y.-L. Liang, M. Khoshouei, G. Deganutti, A. Glukhova, C. Koole, T. S. Peat, M. Radjainia, J. M. Plitzko, W. Baumeister, L. J. Miller, et al., *Nature* **2018**, *561*, 492 – 497.
[37] Y.-L. Liang, M. Khoshouei, M. Radjainia, Y. Zhang, A. Glukhova, J. Tarrasch, D. M. Thal, S. G. B. Furness, G. Christopoulos, T. Coudrat, R. Danev, W. Baumeister, L. J. Miller, A. Christopoulos, B. K. Kobilka, D. Wootten, G. Skiniotis, P. M. Sexton, *Nature* **2017**, *546*, 118 – 123.
[38] M. Wehmer, T. Rudack, F. Beck, A. Aufderheide, G. Pfeifer, J. M. Plitzko, F. Förster, K. Schulten, W. Baumeister, E. Sakata, *Proc. Natl. Acad. Sci. USA* **2017**, *114*, 1305 – 1310.

Manuscript received: February 19, 2019
Accepted manuscript online: March 28, 2019
Version of record online: June 18, 2019

© 2019 Wiley-VCH Verlag GmbH & Co. KGaA, Weinheim